Hygienic Design: Effect of Hydrodynamics on the Cleanability of a Food Processing Line

Walid Blel, Patrick Legentilhomme, Jack Legrand, Thierry Bénézech, Caroline Le Gentil-Lelièvre

AIChE

Hygienic Design: Effect of Hydrodynamics on the Cleanability of a Food Processing Line

W. Blel, P. Legentilhomme, and J. Legrand
Université de Nantes, CNRS, GEPEA, UMR 6144, CRTT, Boulevard de l'Université, BP 406, F-44602 Saint-Nazaire Cedex, France

T. Bénézech and C. Le Gentil-Lelièvre
INRA, UR638, 369 rue Jules Guesde, BP 20039, F-59651 Villeneuve d'Ascq Cedex, France

DOI 10.1002/aic.11559
Published online July 28, 2008 in Wiley InterScience (www.interscience.wiley.com).

Hydrodynamic effect on the numbers of adhering Bacillus cereus spores before and after cleaning in place of part of a dairy processing line was investigated using nonintrusive flow characterization (local wall shear stresses and velocity profiles measurements). Geometrical changes, like gradual asymmetric pipe contractions and pipe expansions and bends, induce nonhomogeneous distribution of the initial and the residual soiling levels. Moreover, the recirculation zone resulting from the flow detachment after the expansion, allowed to explain the high level of adhered spores downstream of this geometrical change due to the generated shear stresses. The resistance to cleaning processes in the same zones is mainly governed by the adhesion strength of spores induced by the applied flow rate in the contamination step. Welding and gasket areas, located at different positions in the loop, constituted deposit spots for spores and remained difficult to clean despite high-shear stress forces involved. © 2008 American Institute of Chemical Engineers *AIChE J,* 54: 2553–2566, 2008
Keywords: Bacillus cereus spores, cleaning, electrochemical method, food safety, hydrodynamics, velocity profiles, wall shear stress

Introduction

Recently, work on cleaning in place (CIP) processes has been done extensively, especially on food related fouling and biofilm in dairy processing lines.[1–3] In present, considerable progress is made in the reduction of fouling. However, few studies investigate hydrodynamic effects on adhesion and detachment of microbial cells or spores on equipment surfaces, even though deposition and attachment of bacterial cells are the first steps in microbial colonization of surfaces in the food industry. Thereafter, biofilm is formed and develops.[4,5] The increase of bacteria levels in the product during processing is partly the result of the release of adhered bacteria that have grown on the equipment walls, in addition to the bacteria grown in the processed product itself.[6,7]

Among the pathogen spore-forming bacteria, *Bacillus cereus* is a public health hazard widespread in nature and frequently isolated from dairy products and equipment. Moreover, *Bacillus cereus* spores are surrounded by an exosporium and long appendages, both inducing a strong adhesion to stainless steel materials.[5,8] Moreover, these spores are known to firmly adhere to a wide variety of materials used in food production equipment,[9] and exhibit a high resistance to heat treatment and standard CIP procedures.[10,11]

Hydrodynamic effect is a major parameter in cleaning processes due to fluid shear forces near the wall.[12,13] In addi-

Correspondence concerning this article should be addressed to C. Le Gentil-Lelièvre at caroline.legentil@lille.inra.fr.

Table 1. Flow Parameters of the Used Solutions

Flow rate	Density (10^3 kg.m^{-3})	η (10^{-3} Pa.s)	Pipe diameter = 3.55×10^{-2}m			Pipe diameter = 2.30×10^{-2}m		
			Re	$V_{average}$* (m.s^{-1})	Blasius value (Pa)	Re	$V_{average}$* (m.s^{-1})	Blasius value (Pa)
300 L.h^{-1} at 20 °C	1.028	0.985	3100	0.08	0.039	5000	0.2	0.19
2200 L.h^{-1} at 60 °C	1.028	0.514	39000	1.05	3.26	60000	2.5	16.6

*Mean velocity calculated for the same Reynolds numbers of cleaning experiment and for a temperature of 20°C (corresponding flow rate 3740 L.h^{-1}).

tion, heat and mass transfer to the wall also contribute in the generated wall shear forces according to the applied flow rate (the momentum transfer). Thus, the efficiency of cleaning rate and microbial removal from the surface is a result of these factors combination.[14] Food processing equipment should be designed and built to ensure hygiene of the production line and then of the products. Furthermore, the hydrodynamic forces (i.e., flow patterns) that affect soil removal from the walls are strongly connected to, especially, the geometrical design of the equipment.[14–16] In various industrial applications, sudden or gradual contraction or expansion pipes and bends are the most widely used geometries. These diameter changes are needed for the installation of various transducers (manometers and flowmeters). Vujičić and Crnojević[17] showed that the flow arrangement after an axis-symmetrical diffuser is widely influenced by the opening angle and the length of this geometry. In addition, it was shown that the stream cross-section changes, resulting from this type of geometry, induce a flow disturbance throughout the downstream production line.[18] Due to the link between cleanability and flow arrangement inside pipes, several studies were made in order to explain the cleanability level upstream and downstream of this type of geometry.[13–15] It was shown that the flow arrangement is less disturbed after a gradual expansion than a sudden one. In both cases, the section change creates a recirculation zone induced by the streamline separation from the wall.[19] However, a good level of cleanability was found in gradual axis-symmetric expansions at low-opening angle, due to the contribution of the fluctuating shear rate in addition to the mean value of wall shear stress to the removal of bacteria.[14,15]

The aim of this study is to investigate the effects of flow characteristics on deposition and detachment of *Bacillus cereus* spores on surface of pieces of equipment representing a section of a dairy production line. In the first part, flow arrangement was investigated by instantaneous velocity profiles (the ultrasonic Doppler velocimetry method) and wall shear stress components (the electrochemical method) at different positions of the loop. The first part makes it possible to explain differences in initial and residual levels of contamination throughout the test loop, based on the flow characteristics. In order to obtain the same Reynolds numbers as during contamination and cleaning experiments, the flow rate was recalculated by considering physical characteristics for the used solutions (Table 1). In the second part, the measured numbers of adhering spores before and after cleaning (initial and residual) are explained using the wall shear stress distributions explained in the first part.

Materials and Methods

Setups

Measurements were carried out in different geometrical configurations (Figure 1) made of 304L stainless steel (2B bright annealed finish; $R_a = 0.3 \pm 0.05$ μm). The test loop was built by an equipment supplier to be close to conditions occurring in dairy processing lines, like the arrangement and the dimension of different pieces of equipment, the position and the type of welding zones. Welding type TIG (Tungsten Inert Gas), 3 mm in width, was made under a mixture of Argon and Nitrogen gas. This mixture is often applied in food industry and allows to obtain a flat welding. Passivation treatment was then applied and ensures the corrosion resistance of the welding. The test loop is formed by a horizontal and a vertical line connected by a bend with coil curvature equal to 56 mm. The diameter changes throughout the test loop were made by gradual asymmetric contraction or expansion pipes located upstream and downstream of an electromagnetic flowmeter (Krohne, OPTIFLUX 6000) with a circular cross-section corresponding to 2.30×10^{-2}m in inner diameter. Two pipe diameters were used (3.55×10^{-2}m and 2.30×10^{-2}m). The parameter H, commonly used as the axial dimensionless coordinate for loops with diametrical change, was defined as the difference between the two diameters. In this work, the value of H is 1.25×10^{-2}m.

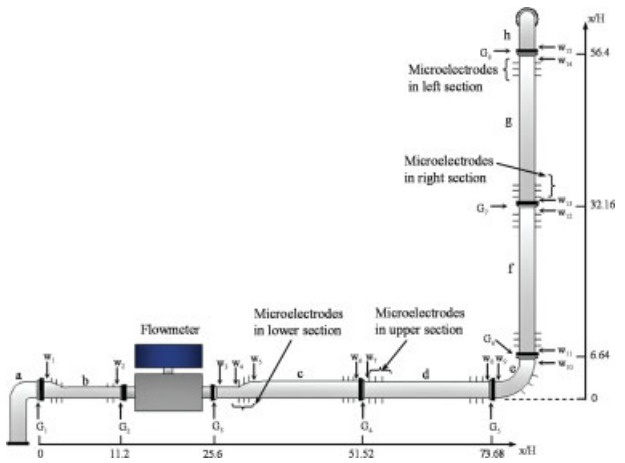

Figure 1. Test loop (W = welding zone; G = gasket).

[Color figure can be viewed in the online issue, which is available at www.interscience.wiley.com.]

Local wall shear stress measurements

Local wall shear stress measurements were done using the electrochemical technique, which consists in measuring the limiting diffusional current given by a redox reaction occurring at the surface of microelectrodes flush-mounted inside the different sections of the test loop (Figure 1). The limiting diffusional current is obtained in a potential range for which the current at the electrode is only controlled by diffusion-convection flux of the reacting species toward the wall. This method allows the instantaneous local mass-transfer coefficient between the electrochemical solution and the microelectrodes to be calculated. Due to the existing analogy between mass and momentum transfers, Reiss and Hanratty[20] proposed a relation between the instantaneous limiting current $I(t)$, given in the dimensionless form of the instantaneous Sherwood number $Sh(t)$, and the shear rate at the surface of the electrode $S_{lev}(t)$, which is known as the "Levêque solution"

$$S_{lev}(t) = \frac{D}{l_e^2}\left(\frac{Sh(t)}{0.807}\right)^3 \tag{1}$$

where l_e is the equivalent length of the working electrode, and D the diffusion coefficient of the active species. However, for high-frequency fluctuating flows, the Levêque solution cannot predict the real wall shear rate. The concentration boundary layer inertia cannot be neglected, and the quasi-steady state assumption is not valid.[21] An attenuation of the signal fluctuation and a phase shift are observed.[22] Sobolik et al.[23] have introduced another technique, based on the correction of the wall shear rate obtained by the Levêque solution by adding a term deduced from the transient response of a probe multiplied by the time derivative of the mass-transfer rate. This method correctly predicts the wall shear rate for high-average Péclet numbers Pe, when the sampling rate is sufficient. These conditions are respected, thus, the wall shear rate method of Sobolik et al.[23] is used in this study and described by the following equation

$$S_{sob}(t) = S_{lev}(t) + 1.204\frac{\partial Sh(t)}{\partial t} \tag{2}$$

The instantaneous value of the wall shear stress $S_{sob}(t)$, is represented as the sum of an average value $\overline{S}$, and a fluctuating value $s(t)$

$$S_{sob}(t) = \overline{S} + s(t) \text{ with } \overline{s(t)} = 0 \tag{3}$$

The wall shear rate multiplied by the fluid viscosity η, gives the average local wall shear stress

$$\tau_w = \eta\overline{S} \tag{4}$$

The shear rate fluctuation *FRS*, was calculated owing to an integration of the power spectral density psd, of the wall velocity gradient, and is defined as follows

$$FRS = \frac{\sqrt{\overline{s^2}}}{\overline{S}} \tag{5}$$

Although the fluctuations of the velocity gradient are filtered by the diffusional boundary layer at the active surface, the onset of the velocity gradient and fluctuations of the limiting current is qualitatively analogous.[24] According to Deslouis et al.[25] when the electrode length increases, the psd decreases, especially in the low-frequencies domain. Therefore, the *FRS* decreases too. Moreover, the used microelectrodes consisted of cross-sectioned platinum wire 1 mm in dia., the *FRS* obtained with these probes were, thus, corrected *via* Deslouis et al.[25] correction factor obtained according to Eq. 6, which presents the ratio between the measured fluctuating shear rate and the actual one

$$\frac{\overline{s^2}\ measured}{\overline{s^2}\ true} = \frac{\Lambda_{fz}^+}{L^+}\,erf\left(\frac{L^+\sqrt{\pi}}{2\Lambda_{fz}^+}\right) \tag{6}$$

Λ_{fz}^+ is the integral correlation length obtained by the integration of the correlation function

$$f(z^+):\ \Lambda_{fz}^+ = \int_0^{z+} f(z^+)dz^+ \tag{7}$$

z^+ corresponding to the value where $f(z^+)$ becomes negative.

The *FRS* correction method is derived from Uberoi and Kovasznay[26] equation, used to treat the data given by a hot wire anemometer having a length larger than the size of the smallest investigated eddies in a given flow, and validated for electrochemical wall shear rate measurements for an upper limit of Λ_{fz}^+ equal to 35.[25] This condition is verified in this work.

In this study, microelectrodes are spaced too far apart, thus, the spatial correlation which allows to calculate the integral correlation length cannot be performed. According to the Taylor hypothesis, the time and spatial correlations can be similar. Therefore, the integral length is deduced from the integral time obtained by the integration of the autocorrelation function, and by using the mean velocity of the fluid.

The electrolytic solution was a mixture of potassium ferricyanide (10^{-3}mol.L^{-1}), potassium ferrocyanide (5×10^{-2}mol.L^{-1}), and sodium hydroxide (0.5 mol.L^{-1}). The density of this solution is 1.028×10^3 kg.m^{-3}, and its dynamic viscosity is 0.985×10^{-3} Pa.s at 22°C. The diffusion coefficient of ferricyanide ions was measured with a rotating disk electrode, the value obtained at 22°C is 3.23×10^{-10}m^2.s^{-1}. The involved electrochemical reaction at the microelectrodes surface is the reduction of the ferricyanide ions

$$Fe(CN)_6^{3-} + e^- \rightarrow Fe(CN)_6^{4-}$$

Experimental values have been compared to the theoretical wall shear stress in a fully-developed turbulent flow, deduced from Blasius' equation (Table 1).[27] In addition, according to Deslouis et al.[25] the fluctuating shear rate at the wall for fully developed turbulent flow is equal to 30% ± 0.02, obtained by different measurement techniques. Thus, the fluctuating shear component was discussed compared to this value.

Velocity profile measurements

The ultrasonic Doppler velocimetry measuring method has been developed for nonintrusive local measurements of fluid

velocities through nontransparent channels of different materials.[28] Instantaneous velocity profiles were, thus, determined at specific positions of the test loop.

The flow measurement system is composed of the DOP 1000 multigate ultrasonic velocimeter, and an ultrasonic transducer (the basic frequency of ultrasound is equal to 4 MHz) both from Signal Processing S.A. (Lausanne, Switzerland). The average diameter of the microparticles suspended in the liquid used as tracer is approximately 80 μm (microcapsules of oil having a density close to that of water).

The principle of Doppler ultrasonic technique consists in the emission of an ultrasound beam from a transducer; the ultrasound wave is scattered by the moving particles and partial backscattered ultrasound is then received by the same sensor probe.

The particle location is obtained from the time duration between the pulse emission and the echo detection. At the same time, the velocity information V, is derived from the Doppler shift frequency[28]

$$V = \frac{Cf_D}{2f\,cos(\theta)} \tag{8}$$

where C is the ultrasound velocity, f_D the Doppler frequency, f the ultrasound frequency, and θ the Doppler angle.

The axial velocity profile is obtained at each axial measurement position. However, even for a fully-developed turbulent flow, the instantaneous velocity is three-dimensional (3-D), and the particles present a fluctuating velocity in the radial and the tangential directions in addition to the mean and the fluctuating axial velocity. This problem can be solved by averaging enough velocity profiles.[29] In this work, 512 velocity profiles have been averaged at each position. Thus, instantaneous velocity profiles can be denoted by

$$v(\vec{x},t) = V(\vec{x}) + v'(\vec{x},t) \tag{9}$$

$V(\vec{x})$ is the average velocity, $V'(\vec{x},t)$ is the fluctuating velocity, and t is the acquisition time.

The turbulence intensity in the axial direction is defined as

$$Tu = \frac{\sqrt{\overline{v'^2}}}{V} \tag{10}$$

Amount of adhering spores before and after cleaning process

The level of adhering spores was investigated before and after cleaning. In the first case, the processing line was soiled and rinsed, contamination levels are then determined. In the second case, the hygienic status of the test configuration was investigated by means of the number of residual adhering spores, after a complete run of soiling and cleaning.

The soiling step of the test loop was performed under dynamic conditions by 1 h at 300 $L.h^{-1}$, and at room-temperature, of *Bacillus cereus* CUETM 98/4 spores (Collection Unité Ecotoxicologie, Villeneuve d'Ascq, France) suspended at 10^3 $CFU.mL^{-1}$ in water. This concentration allows good observation of soiling levels. This strain was isolated from an industrial dairy processing line. It was chosen for its ability to adhere firmly to stainless steel, and its high resistance to CIP procedures.[9] The test loop was then rinsed in place for 5 min at 300 $L.h^{-1}$ with softened water at room-temperature.

To determine residual contamination after CIP (hygienic status) a similar soiling step at 10^5 $CFU.mL^{-1}$ suspended spores in water and the same rinsing step was performed. Then, cleaning was performed with sodium hydroxide (0.5% w/w) at 60°C for 10 min at 2,200 $L.h^{-1}$. Finally, the test loop was rinsed for 5 min with softened water at 600 $L.h^{-1}$.

Evaluation of the initial and the residual soiling levels was carried out separately for the two types of experiments using a tetrazolium chloride (TTC) agar overlay technique.[30] Each section was half-filled vertically with TTC agar and incubated horizontally for 4 h at room-temperature. Then, the molded agar was gently detached from the steel surfaces, extracted from the pipe, and then further incubated for 20 h at 30°C. *Bacillus* colonies, appearing in red, were distinguishable at the mold surface and distributed according to the position of the adhered spores at the inner wall of pipes. Three trials were carried out for the initial contamination experiment, and four for the residual one. For each type of experiments (initial or residual contamination), different zones of equipment were determined according to the density of colonies present at the surface. In order to improve the contamination levels characterization of equipment, a high number of zones with small surfaces area are defined for each geometry. A statistical analysis was then performed to map the contamination level observed on the walls of the test equipment.[31] This statistical treatment was carried out separately to evaluate the initial and the residual levels of contamination. For each geometry, the contamination level was given at the upper and the lower sections of the horizontal part, and the left and the right sections of the vertical one (hemi-cylindrical molding). Physical properties of the fluid used in this study are shown in Table 1.

Surface topography and roughness measurements

In order to correlate the surface properties to spores adhesion levels, as well as the local flow disturbance, surface topography and roughness measurements were made in some critical zones (especially welding zones located at the end of the test pipes and before and after diameter changes). The surface characterizations system used is composed of a roughness and waviness measuring instrument (Perthometer S2) controlled by the software MarSurf XR 20, both from Mahr GmbH (Goettingen, Germany).

Surface roughness characterization was made via two parameters. The first is the average roughness R_a (μm) which corresponds to the arithmetic average of the absolute values of the roughness profile ordinates $Z(x)$, deduced from the traced profile of the real surface[32]

$$R_a = \frac{1}{l_s}\int_0^{l_s} |Z(x)|dx \tag{11}$$

The second parameter is the profile depth P_t(μm), which is the sum of the largest profile peak height, and the largest profile valley depth of the P-profile computed from the traced profile.[32]

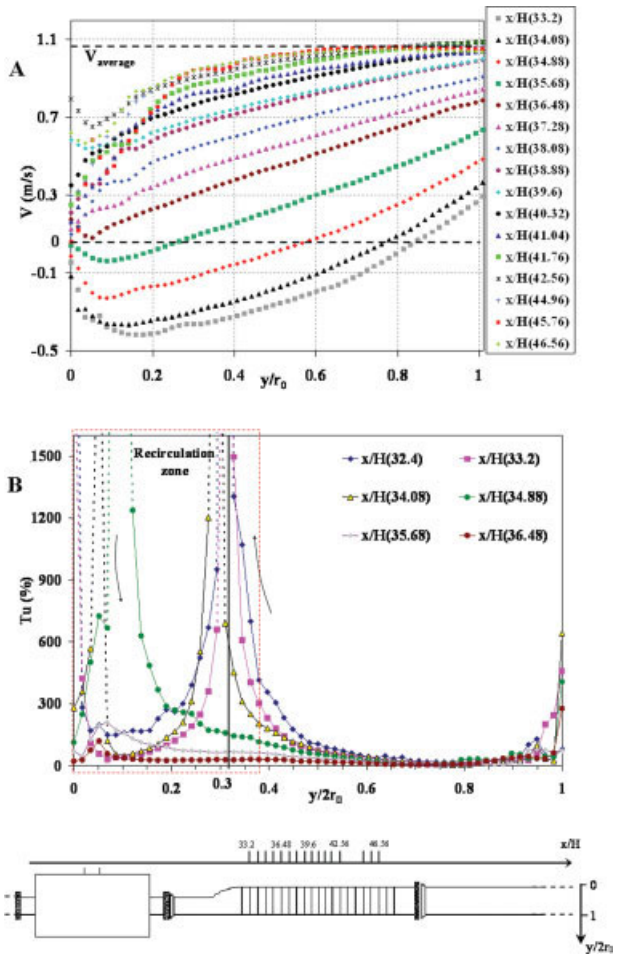

Figure 2. Velocity profiles at the upper section (A), and turbulence intensity (B) measured at different positions x/H of part "c" after the expansion (Re = 60,000 for 2.30 × 10^{-2}m pipe dia.).

[Color figure can be viewed in the online issue, which is available at www.interscience.wiley.com.]

Experimental results and analyses

To study the hydrodynamic effects on the initial and residual levels of adhering spores, soiling and cleaning experiments, and flow characterization were carried out at different positions of the test configuration (Figure 1).

Geometry effect on the flow arrangement

Flow behavior inside pipes is a determining element in the wall shear stress distribution, which constitutes a key factor in the bacterial removal. For this reason, flow analysis in this part was performed for only the same flow rate used in the cleaning tests.

Figure 2A illustrates the evolution of velocity profiles after the expansion. Negative velocities are recorded at the top of the geometry and cover the entire zone after the expansion until x/H close to 36.5 (Figure 2A).

According to Vujičić and Crnojević,[17] the position of the separation point of the boundary layer near the wall depends on the angle of the diffuser and on the Reynolds number. The increase of the flow section due to the high-opening angle of the expansion (35.9°), in addition to the highest Reynolds number tested (60,000 for 2.30 × 10^{-2}m pipe dia.), induces a fluid jet separated from the wall, and, thus, creates a recirculation zone, which rotates in the opposite direction of the flow (Figure 2A). In addition, Figure 2B showed high-turbulence intensities at the same zone. This result can be explained by the high vorticity of rotating fluid downstream of the expansion. Flow direction is shown in this zone. Dashed lines for each position correspond to the recirculation zone border. Downstream the expansion ($32.4 < x/H < 33.2$), recirculation zone bound can be estimated at $y/2r_0 = 0.32$ (Figure 2B), and decreases throughout the pipe until the reattachment point of the new boundary layer.

The slope of the mean velocity profiles at the upper pipe wall $((\partial v/\partial y)_{y=0})$ from the position x/H = 36.48 (Figure 2A) reveals smooth gradient, which corresponds to low-friction velocity (V^*), according to the following equation

$$V^{*2} = \frac{\eta}{\rho}(\partial v/\partial y)_{y=0} \tag{12}$$

Thus, low-theoretical mean wall shear stresses exist at this position, corresponding to the reattachment point of the new boundary layer, and increase through the geometry. Figure 3 illustrates the effect of the boundary layer development on the velocity profiles shape near and far from the expansion, and allows to suppose an important shear stress variation throughout this geometry.

After the expansion, the flow evolves toward the fully-developed state and the length to obtain fully-developed flow can be obtained using the velocity profile measurements. Figure 4 illustrates the evolution of normalized velocity profiles at different positions x/H throughout part "d" and following

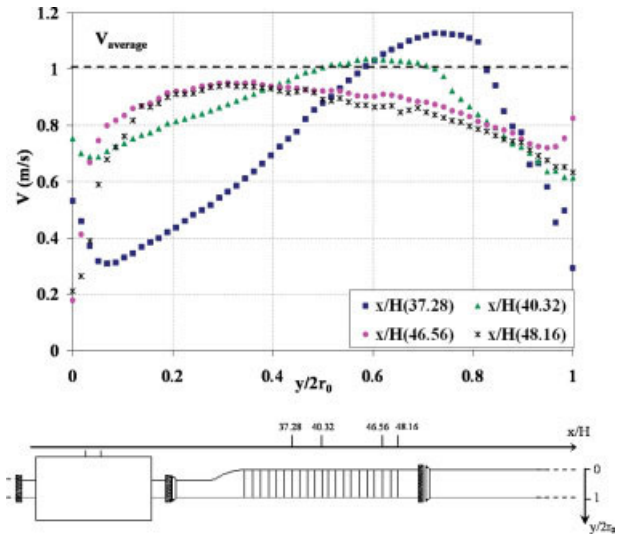

Figure 3. Nondimensional velocity profiles evolution measured at different positions x/H of part "c" after the expansion (Re = 60,000 for 2.30 × 10^{-2}m pipe dia.).

[Color figure can be viewed in the online issue, which is available at www.interscience.wiley.com.]

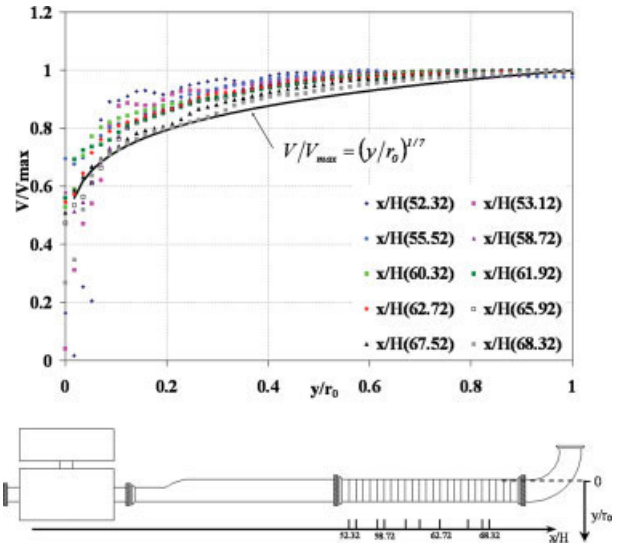

Figure 4. Evolution of experimental and theoretical velocity profiles in part "d" (Re = 60,000 for 2.30 × 10^{-2}m pipe dia.).

[Color figure can be viewed in the online issue, which is available at www.interscience.wiley.com.]

the half longitudinal coordinate (y), normalized by the pipe radius (r_0). Comparison was made with the 1/7 power law, which constitutes a good approximation for the turbulent core region.[27] The velocity profile at the position x/H = 68.32 is very close to the 1/7 law (maximum difference of 0.6%), and shows that the mean flow can be considered as fully-developed at this position.

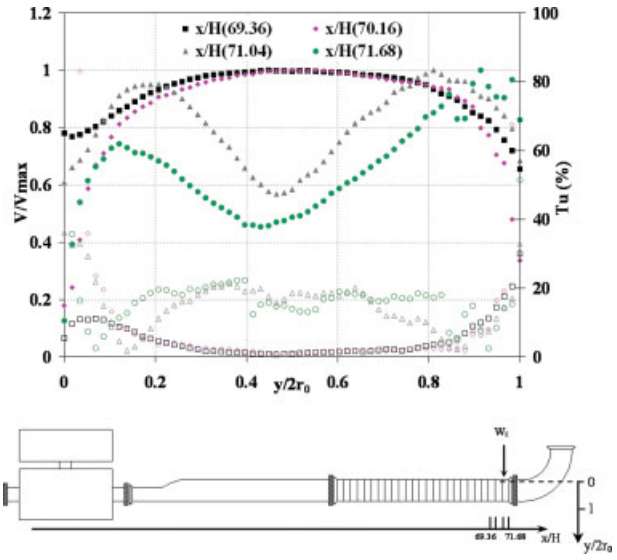

Figure 5. Velocity profiles (filled symbols) and turbulence intensity (empty symbols) measured at the end of part "d" (Re = 60,000 for 2.30 × 10^{-2}m pipe dia.).

[Color figure can be viewed in the online issue, which is available at www.interscience.wiley.com.]

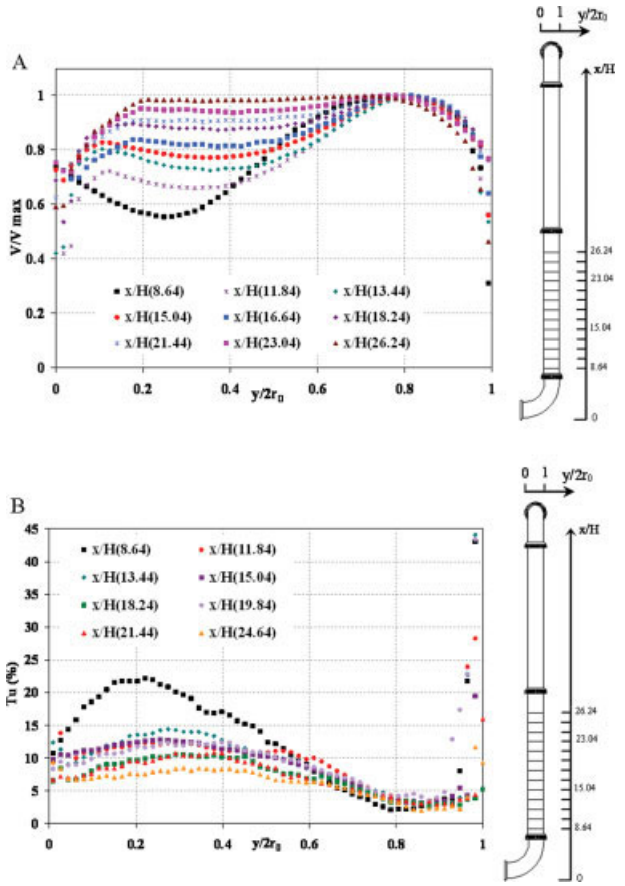

Figure 6. Nondimensional velocity profiles (A), and turbulence intensity (B) evolution measured at different positions x/H of the vertical line (Re = 60,000 for 2.30 × 10^{-2}m pipe dia.).

[Color figure can be viewed in the online issue, which is available at www.interscience.wiley.com.]

The velocity profiles close to the gasket and the welding zones exhibit an important disturbance and a significant attenuation of the velocity values along the axial flow direction (Figure 5). The direction change induced by the curved edge of the bend can also explain this flow deceleration. However, the attenuation along the axial direction is compensated by the radial and the tangential components in order to keep the same flow rate. Positive values of the mean velocity at these surface irregularities reveal a nonboundary layer detachment from the wall, but only a flow disturbance occurs, which explains high-turbulence intensities observed at these zones (Figure 5).

Throughout the vertical line, 1-D velocity profiles evolution after the bend (Figure 6A) shows that maximum values no longer occur at the tube centerline, but nearer the wall at the convex wall of the bend. The pressure increase in the vicinity of the external wall and decrease close to the inner wall[33] could explain these observations.

A high Dean number value for the two flow rates of contamination and cleaning experiments (D_n = 1,750 and 21,760, respectively) indicates the presence of secondary flow patterns in which fluid flows outward from the center of

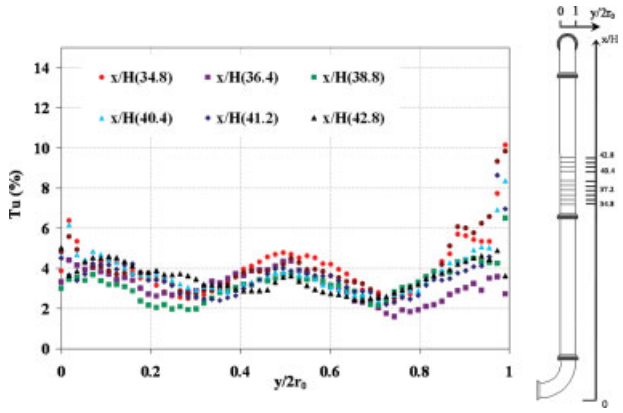

Figure 7. Turbulence intensity measured at different positions x/H along the straight pipe "g" (Re = 60,000 for 2.30 × 10^{-2}m pipe dia.).

[Color figure can be viewed in the online issue, which is available at www.interscience.wiley.com.]

the pipe to the convex wall of the bend (right section in Figure 1), and then around this area in a pair of cells often called contrarotating Dean roll cells. Centrifugal forces induced by these Dean cells generate high-turbulence intensities (Figure 6B) observed near the left wall.

The non-established flow persists at the beginning of the straight pipe "g", and can be confirmed by the turbulence intensities (Figure 7), which present nonconstant values at the core of the pipe, and lower than 30% at the wall.

The length to obtain fully developed flow after the bend was examined via velocity profiles when the boundary layer is entirely developed. Indeed, at the position x/H = 54, experimental nondimensional velocity is very close to the 1/7 power law profile throughout the nondimensional radius (Figure 8).

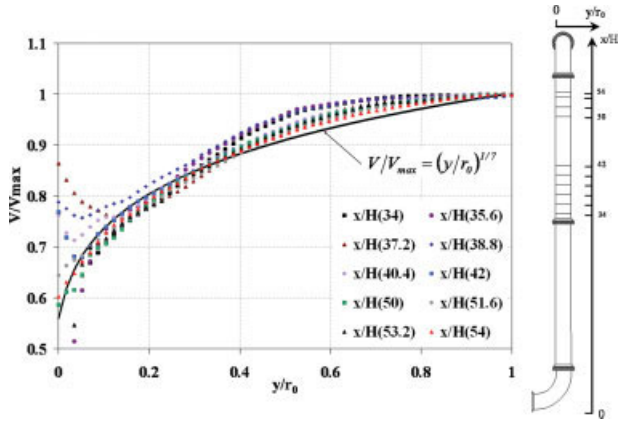

Figure 8. Evolution of experimental and theoretical velocity profiles in the straight pipe "g" (Re = 60,000 for 2.30 × 10^{-2}m pipe dia.).

[Color figure can be viewed in the online issue, which is available at www.interscience.wiley.com.]

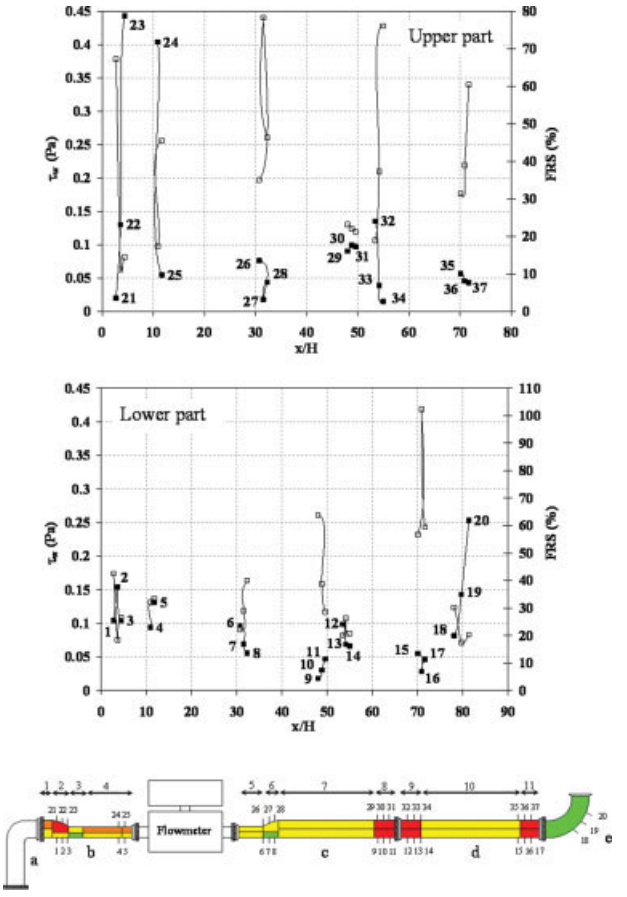

Figure 9. Wall shear stress and mapping of adhering spores measured at the upper and the lower sections of the horizontal line (Re = 5,000 for 2.30 × 10^{-2}m pipe dia.), with *FRS* (□) and τ_w(■).

In green, the poorly soiled zones, in yellow, the moderately soiled zones, in orange, the soiled zones and in red, the highly soiled zones. [Color figure can be viewed in the online issue, which is available at www.interscience.wiley.com.]

Analyses of the bacterial contamination before and after cleaning: role of the flow arrangement

In this part, soiling and cleaning experiments and electrochemical measurements were carried out separately on two sides of the test configuration, the top or the bottom of the horizontal line and the left or the right part of the vertical one (Figure 1).

Analysis of the Initial Level of Adhering Spores Before Cleaning. The soiling levels of adhering spores were classified in four groups varying from the poorly soiled zones to the highly soiled ones (Figures 9 and 10).

- Gradual contraction (noted "b" in Figure 9)

The flow rate used in soiling experiments was selected to mimic the circulation of food products during production process (Re = 5,000). Wall shear stress variations at the upper and the lower parts of the zone 2 showed the effect of the interaction between the bend and the gradual contraction

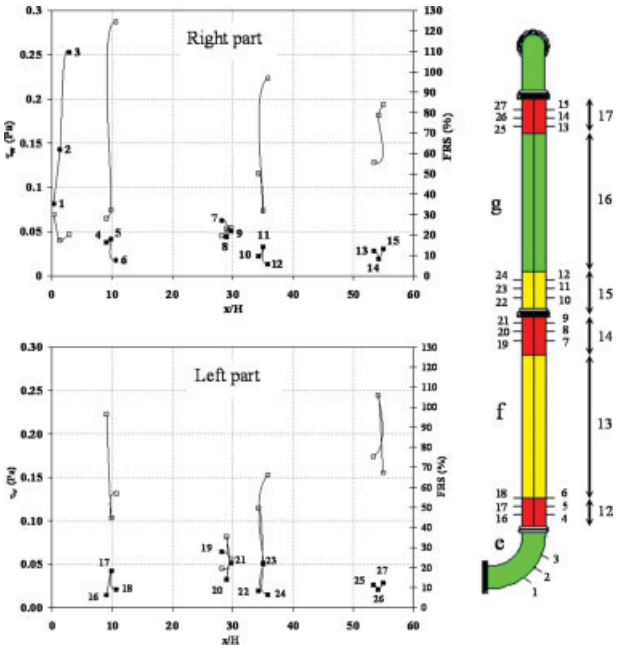

Figure 10. Wall shear stress and mapping of adhering spores measured at both right and left sections of the vertical line (Re = 5,000 for 2.30 × 10^{-2}m pipe dia.), with *FRS* (□) and τ_w(■).

In green, the poorly soiled zones, in yellow, the moderately soiled zones, in orange, the soiled zones and in red, the highly soiled zones. [Color figure can be viewed in the online issue, which is available at www.interscience.wiley.com.]

on the flow pattern at the beginning of the horizontal portion of the loop (Figure 9). Consequently, soiling levels are not homogeneous, and varied from highly soiled zones to poorly soiled ones (the upper and the lower sections of zones 2 and 3, respectively).

Flow disturbance induced by the gradual contraction located at the top of this geometry (zone 2) could explain the high level of contamination at the upper section in comparison with the lower one.

The curved edge of bend "a" located upstream induces a flow disturbance. Indeed, a high Dean number value is observed with the contamination flow rate (D_n = 1,750). Thus, low values of local wall shear stress were observed at the wall, especially for probes P_1 and P_{21} located on the same vertical line (respectively, 0.10 Pa and 0.02 Pa for x/H = 2.72). The increase of the shear stress observed at P_{23} (0.44 Pa) can be explained by the plugging effect caused by the gradual contraction (35.9°) on the flow ejection after the bend curvature.[27] As a result of this plugging effect, an increase of wall shear stress is observed at the middle of the lower part (0.15 Pa at P_2 against 0.10 Pa at P_1 and P_3) due to the pressure increase at the wall.

The diameter change induces high-shear stresses at the beginning of the straight section (zone 3), resulting in a low level of contamination.

The combination of successive effects of the bend and of the gradual contraction on the flow arrangement induces a significant variation of the wall shear stress values at the end of part "b". Alternating maximum and minimum values on probes placed symmetrically along the loop axis emphasize the oscillating behavior of the flow (0.094 Pa for P_4, against 0.403 Pa for P_{24} and 0.131 Pa for P_5, against 0.055 Pa for P_{25}). This alternation of maximum and minimum values was previously observed downstream of other geometrical changes, which induce flow disturbance like the annular swirling decaying flow.[34] However, the mean value of the wall shear stress for these four probes is close to the theoretical value calculated according to Blasius' equation (respectively, 0.17 Pa and 0.19 Pa), which emphasizes the momentum-transfer conservation.

- Gradual expansion (noted "c" in Figure 9).

For part "c", a moderate level of contamination was observed in the upstream section of the expansion (zone 5). This result is mainly due to the high-wall shear stress values throughout this zone (0.097 Pa for P_6 and 0.076 Pa pour P_{26}), in comparison to the average wall shear stress in the entire loop for the applied flow rate (≈ 0.07 Pa), but remains under the theoretical Blasius value (0.19 Pa). Under these flow conditions, the generated shear stress forces appeared to reduce the bacterial adhesion phenomenon. The homogeneous contamination of the surface of this zone could be explained by a combination of the adhesion and the release of loosely bounded spores. Several studies have already shown that the adherence of bacteria can be defined as the sum of the deposition and the parts released as a result of shear.[4,35–37]

The gradual expansion of this geometry (zone 6) was found to be moderately soiled at the upper section and poorly soiled at the lower one. However, low values of local wall shear stress were observed (0.018 Pa for P_{27} and 0.056 Pa for P_8) in comparison to the theoretical fully-developed flow value for a pipe diameter of 2.30 × 10^{-2}m (0.19 Pa), but the fluctuation shear rates were high enough, at both lower and higher sections (40% for P_8, between 30 and 78% for probes P_{26}, P_{27} and P_{28}), to significantly contribute to the removal of spores after adhesion. The expansion angle close to 35.9° is high enough to induce streamlines separation from the wall, and, thus, recirculation zone theoretically characterized by mean wall friction forces close to zero and high-fluctuation rate.[17] This zone extends beyond the expansion, which explains the moderate contamination level (yellow zone) recorded at both top and bottom behind the expansion (zone 7). Indeed, a homogeneous spores transport from the solution to the wall occurs, but this uniform soiling level of the zone 7 does not mean that spores adhesion force is similar throughout this area. It was proven that adhesion forces depend on the wall shear stress induced by the flow rate.[38–40] At low-shear forces, mass transport to the wall occurs by sedimentation and lower adhesion forces are considered.[39]

Experimental works of De Jong et al.[41] carried out with a rotating disk, have shown the existence of a critical value of the shear stress under which a significant bacteria adhesion phenomenon at the wall occurs, and above which adhesion decreases monotonically with the applied shear stress. In addition, a release of less adhered bacteria occurs, too. Soiling levels (yellow zone in Figure 9), as well as the recirculation zone located after the expansion show that wall shear

Table 2. Surface Characterization Measured on Welding Zones of the Tested Geometries

Geometry	Welding	Side	R_a (μm)	P_t (μm)
b	W_2	top	4.56	249.6
		bottom	1.84	92.5
c	W_6	top	4.57	387.9
		bottom	2.40	182.0
d	W_7	top	3.44	229.7
		bottom	3.64	352.9
	W_8	top	4.40	326.2
		bottom	4.37	255.1
f	W_{12}	left	3.08	218.4
		right	1.87	137.8
g	W_{14}	left	3.88	297.4
		right	3.13	183.7
Far from the welding			0.26	5.0

stresses induced by the flow pattern at this section of part "c" are not high enough to generate strong adhesion forces of spores at the wall.

The end of part "c" presents a high-soiling level at the upper and the lower sections (zone 8). The apparent difference of local wall shear stress values between the two sections could not explain this homogeneous repartition of contamination (around 0.099 Pa for P_{29}, P_{30} and P_{31} against 0.018 Pa, 0.03 Pa and 0.047 Pa for P_9, P_{10} and P_{11}). However, the effect of the gasket and the welding zones can explain this result. Indeed, this effect can be emphasized by surface characteristics, especially the topography which is modified by the existence of the welding zone. This irregularity at the surface presents high P_t values (388 μm at the upper section, and 182 μm at the lower one for W_6), which could induce the creation of an unsteady flow due to the local perturbation of the boundary layer (see Table 2). This result is confirmed by a mean wall shear stress at this zone higher than the theoretical value for a fully-developed flow (0.063 Pa against 0.039 Pa). Moreover, the high-soiling level observed in this zone could be due to the high-surface roughness (4.57 μm and 2.40 μm at the upper, and the lower sections of W_6 against 0.26 μm far from the welding), which constitutes a base for spores adhesion. Indeed, according to Jullien et al.[11] the number of adhering *B. cereus* spores rises with the increase of the average roughness from the standard value of 0.8 μm.

- Straight pipe (noted "d" in Figure 9).

Part "d" showed a high-contamination level up to x/H = 55 (zone 9); the beginning of this geometry also contains a welding zone (W_7) at x/H = 52.9, with high-surface roughness (respectively, 3.44 μm, and 3.64 μm at the upper and the lower sections) in comparison with the standard value of 0.8 μm recommended by the standard,[32] which confirms the effect of these irregularities on adhesion of spores. Local wall shear stresses measured at the upper section are even higher than at the lower one, as a result of the important momentum-transfer rate due to a not-fully-developed flow at the upper section of this nonaxisymmetric expansion, whereas the boundary layer at the lower section is weakly disturbed. The comparison between wall shear stresses close to welding zones of the different geometries and P_t values (Table 2), used to explain the flow disturbance induced by the surface topography change at the welding area, confirms this observation. Results observed upstream and downstream of the gasket located between geometries "c" and "d" showed that the level of contamination in this zone is independent of shear stresses and that it is mainly related to surface characteristics.

For $55 \leq$ x/H ≤ 70.5 (zone 10), the same soiling level at the upper and the lower sections is observed. Close values of wall shear stress were recorded for the two sections, especially at the end of this zone (0.055 Pa and 0.057 Pa, respectively, for P_{15} and P_{35}). This result shows that the flow becomes symmetrical after an establishment distance upstream of the expansion. However, the boundary layer cannot be considered as fully-developed, given that the mean shear stress at this position, from which the flow becomes axis-symmetric, is higher than the theoretical value (0.056 Pa against 0.039 Pa).

The end of the geometry (zone 11) is highly soiled at both the upper and the lower sections. Gasket and welding effects allow to explain this result in addition to the role of the curved edge of the bend localized upstream of this zone, which induces the deceleration of the flow owing to the direction change.

- Bend (noted "e" in Figure 9).

The low-soiling level observed at the bend is due to the high values of wall shear stress recorded at the external wall of this geometry (0.082 Pa at P_{18}), and which increases throughout the geometry (0.143 Pa at P_{19} and 0.253 Pa at P_{20}). These values can be considered very high in comparison with the supposed spores adhesion forces.[42]

- Straight pipes located downstream of the bend (noted "f" and "g" in Figure 10).

For the vertical line, zones 12, 14 and 17 present a high-soiling level (Figure 10). Welding and gasket located upstream or downstream of these zones induce flow disturbances characterized by high-fluctuation shear rates (96%, 35 and 105%, respectively, for P_{16}, P_{20} and P_{26}).

Zone 13 is moderately soiled. Flow pattern in this section is largely influenced by the bend which induces a local flow disturbance verified by the high Dean number (D_n = 1,750). This flow disturbance disappears after an establishment length. Indeed, a homogeneous contamination level is observed throughout zone 16, and could be explained by the high level of shear stresses generated by this flow pattern. The flow establishment can also explain the moderate soiling level of the zone 15 in comparison with the other extremities of pipe "f" and "g" (zones 12, 14 and 17). The decrease of contamination levels throughout these two pipes, following the flow direction, can confirm this observation (zones 12 and 13 for the pipe "f" and zones 15 and 16 for the pipe "g").

To summarize, soiling experiments showed that adhesion of *Bacillus cereus* spores on the surface seems to be governed mainly by the intensity of mean and fluctuating shear stress which determine the contribution of sedimentation, convection and diffusion in transport processes of spores. The flow rate is a determining parameter in this transport phenomenon from the solution to the surface. Moreover, adhesion forces at the wall depend on this parameter. The same observations have been done by Faille et al.[43] for various flow conditions.

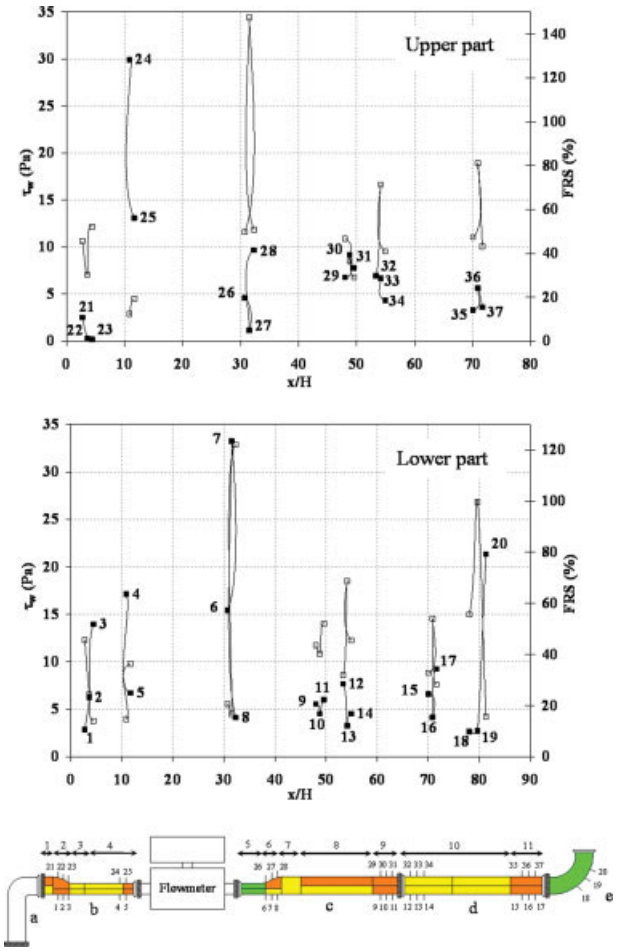

Figure 11. Wall shear stress and mapping of the residual adhering spores measured at the upper and the lower sections of the horizontal line (Re = 60,000 for 2.30 × 10^{-2}m pipe dia.), with *FRS* (□) and τ_w (■).

In green, the correctly cleanable zones, in yellow, the cleanable zones and in orange, the moderately cleanable zones. [Color figure can be viewed in the online issue, which is available at www.interscience.wiley.com.]

In addition, after the gradual expansion, transport and adhesion of spores to the wall depend on the swirling intensity in the recirculation zone which is tributary of the opening angle of the expansion and the Reynolds number. Finally, a high amount of adhering spores is observed at gasket and welding zones, which constitute deposit spots for spores, and, therefore, in that case could govern the soiling levels observed.

Analysis of the Residual Level of Adhering Spores after Cleaning. The cleaning step was performed with sodium hydroxide at 60°C for 10 min at 2,200 L.h^{-1}. The residual soiling levels of adhering spores after cleaning were classified in four different groups varying from the correctly cleanable zones to the poorly cleanable ones (Figures 11 and 12). Global observation emphasizes that the horizontal line is poorly cleanable in comparison with the vertical portion.

- Gradual contraction (noted "b" in Figure 11)

The flow arrangement in part "b" is largely influenced by the interaction between the bend "a" and the gradual asymmetric contraction. This effect induces a nonhomogeneous repartition of wall shear stresses at the upper and the lower sections (13.95 Pa, 2.51 Pa and 0.27 Pa, respectively, at P_3, P_{21} and P_{22}). However, the homogeneous residual contamination observed at zones 1 and 2 can be explained by the high-residence time of the cleaning solution in this section of the geometry, due to the recirculation zone induced by the bend curvature and the contraction. A beneficial effect of this contraction is observed in the straight portion (zones 3 and 4), which presents a good level of cleanability due to the high-shear stresses.

Shear stress values at the end of this geometry drop significantly at both sides (13.09 Pa at P_{25} against 29.93 Pa at P_{24}, and 6.72 Pa at P_5 against 17.13 Pa at P_4). The flowmeter mounted between two couplings can explain the wall shear stress drop at P_5 and P_{25}, and, thereafter, the observed moderate level of cleanability at the end of this geometry. However, the mean value of wall shear stress for these four probes is similar to that calculated according to Blasius' equation (respectively, 16.7 Pa against 16.6 Pa).

- Gradual expansion (noted "c" in Figure 11).

For part "c", the straight pipe before the expansion (zone 5) exhibits a high-cleanability level due to the high-shear stress forces measured at the end of this section (P_6), and which can be considered very close to the theoretical value for this pipe diameter (respectively 15.4 Pa at P_6 against 16.6 Pa). This high-cleanability level can also be explained by the low initial soiling level. In this context, theoretical works of Ziskind et al.[44,45] have shown that particle release should be based on two main factors, namely the interaction between the surface and the particle, and the effect of the flow field on particles, which creates high-shear stresses in the viscous sublayer of the turbulent boundary layer.[45]

Despite the high value of the fluctuation shear rate measured at the probe P_{27} (147%), which be considered more important than the theoretical value for a fully developed turbulent flow (30% ± 0.02),[25] the upper section of the expansion (zone 6) is moderately cleanable, but the mean shear stress is very low (1.16 Pa at P_{27}). Thus, the fluctuating component of the shear stress does not have significant effect on spores detachment if the mean value is too low. Indeed, the positive effect of the mechanical factor on cleanability is the result of the combination of the two wall shear stress components.[15,37,45]

The lower section of the expansion is a cleanable zone. A sudden increase of the mean shear stress is observed between probes P_6 and P_7 (respectively, 15.4 Pa and 33.23 Pa), and can explain the observed cleanability. This result could be induced by the bursting phenomenon of turbulence structures in the near-wall region, probably due to the boundary layer detachment after the expansion.[46] On the other hand, negative velocities are recorded at the top of the geometry, and cover the entire zone 7 up to x/H = 35.7 (Figure 2A). In this same zone, high-turbulence intensities are observed (Figure 2b). Thus, centrifugal forces induced by this flow pattern allow the release of the adhered spores and could explain the cleanability level. This positive effect of velocity fluctuation was already proven theoretically for particles resuspension from several surface roughnesses.[45]

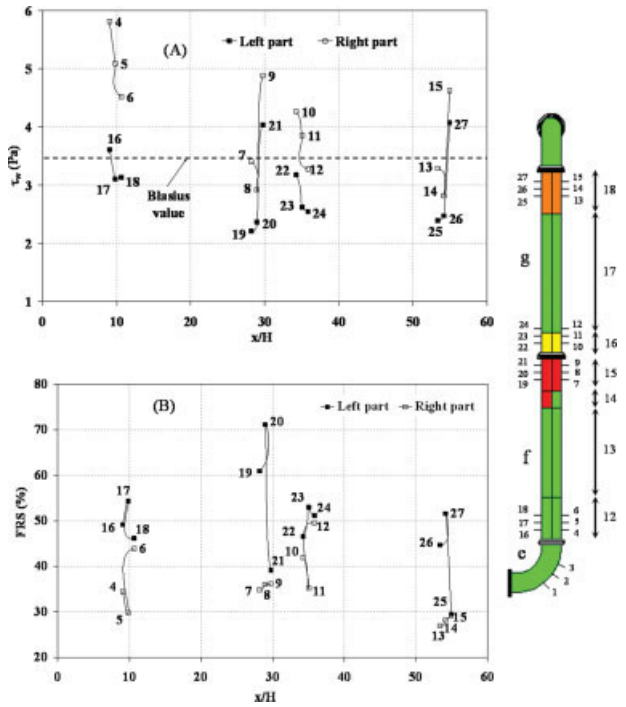

Figure 12. Wall shear stress components (τ_w (A), and *FRS* (B)), and mapping of the residual adhering spores measured at both right and left sections of the vertical line (Re = 60,000 for 2.30×10^{-2}m pipe dia.).

In green, the correctly cleanable zones, in yellow, the cleanable zones, in orange, the moderately cleanable zones and in red, the poorly cleanable zones. [Color figure can be viewed in the online issue, which is available at www.interscience.wiley.com.]

The upper section of zones 8 and 9 (geometry "c") exhibits a moderate level of cleanability. Turbulence intensities near the wall in zone 8 are less important than in zone 7, and monotonically decrease due to the weak recirculation zone activity far from the expansion. Moreover, the flow arrangement at this zone induces low-mean wall shear stresses. These wall shear stresses increases through the geometry, but remain lower than adhesion spores forces.

The lower part of the zone 8 is a cleanable region. Velocity profiles near the lower pipe wall of this zone (x/H = 37.28, and 40.32 in Figure 3) showed maximum values which correspond to a high- friction velocity, according to the Eq. 12, and allow to explain the observed cleanability level.

The variation in the cleanability level between zone 7, and the upper section of zone 8, could be explained by the difference in adhesion forces of spores during the initial step of contamination of the two zones. Indeed, the recirculation zone induced by the gradual expansion occurring during contamination experiment covers the entire zone 7 and ensures spores transport to the wall. However, the resulting shear stresses are low and induce weak adhesion forces. Spores are then easily detached during the cleaning experiment. On the other hand, the upper section of zone 8, localized after the recirculation zone, is theoretically characterized by more important shear stresses than for zone 7, given that the flow is more developed. Thus, spore adhesion forces generated by the contamination flow are higher than those at zone 7, which explains the moderate cleanability level of zone 8. The end of geometry "c" presents high values of wall shear stress at the upper section, in comparison with the theoretical value (6.77 Pa, 9.13 Pa and 7.80 Pa, respectively, at x/H = 48, 48.8 and 49.6 against 3.26 Pa from Blasius' equation). This result is in accordance with velocity profiles at x/H = 48.16 and 46.56, which show maximum fluid velocity at the upper section of part "c" (Figure 3), due to the thinness of the boundary layer formed after the flow disturbances. However, this zone is moderately cleanable at both upper and lower sections. The gasket and the welding present in this zone constitute deposit spots for *B. cereus* spores. The presence of exosporia and appendages together with high roughness of the surface, make bacterial removal difficult. Thus, despite the high-shear stress forces, cleaning is difficult in this zone.

- Straight pipe (noted "d" in Figure 11).

Geometry "d" presents two levels of cleanability. The first section, which extends up to x/H = 68.24, is a cleanable zone. The homogeneous repartition of the residual adhered spores at both upper and lower sections can be explained by the very close values of mean and fluctuating shear stresses recorded at axis-symmetric probes (4.53 Pa and 45.5% against 4.32 Pa and 40.85%, respectively, at P_{14} and P_{34}). Thus, the flow behavior after the expansion tends to become fully-developed, and the establishment length is obtained in the first part. The last section of part "d" is moderately cleanable. In addition to the perturbation due to the gasket and the welding with high roughness (Table 2), direction change of the flow induced by the bend has an effect on the observed cleanability level. A blocking phenomenon caused by the curved edge generates a distorted flow, especially at the lower section, confirmed by high-wall shear stresses measured at P_{17} (9.25 Pa), and which corresponds to a maximum at the convex wall of the bend. However, shear stresses close to the theoretical value were observed at the upper section (3.60 Pa at P_{37} against 3.26 Pa).

- Bend (noted "e" in Figure 11).

The good cleanability level observed at the bend can be explained by the low-initial contamination and the high-wall shear stress values recorded at the external wall (21.32 Pa at x/H = 2.88). Throughout the vertical line, higher values of the shear stress are observed at the right side than at the left side (Figure 12A). In addition, very high fluctuating shear rates are recorded downstream of the curved edge (49%, 54% and 46.1% at P_{16}, P_{17} and P_{18} against 34.4%, 29.8% and 43.8% at P_4, P_5 and P_6), confirming the asymmetric behavior of the flow after the bend analyzed in the first part (Figure 12B).

- Straight pipes located downstream of the bend (noted "f" and "g" in Figure 12).

The straight pipe "f" is correctly cleanable at both left and right sides of zones 12 and 13, due to centrifugal forces induced by the direction change of the flow (described in the first section). The decrease of the contra rotating Dean roll cells activity in addition to the existence of a welding zone,

Table 3. Shear Stress Components Effect on the Cleanability Levels for Different Geometries and Under the Same Flow Rate

Shear stress forces magnitude	Cleanability levels	Geometries	Surface properties
- High mean shear stress - High *FRS*	High	- Diametrical changes (gradual expansion at opening angle lower than7°)[17] - Straight pipes presenting little disturbances of the boundary layer without separation from the wall - Bends with high coil curvature	High surface quality
- High mean shear stress - High *FRS*	Low	- Welding and gasket zones	Low surface quality (high average roughness) for welding and different surface properties and adhesion ability for gasket
- High mean shear stress - Average *FRS*	High	Straight pipes downstream flow disturbances (thinness boundary layer)[27]	High surface quality
- Average mean shear stress - High *FRS*	High	Diametrical changes with average opening angle (7 − 8°)[17]	High surface quality
- Average mean shear stress - Average *FRS*	Moderate	Straight pipe after a long establishment length (up to D × 20)	High surface quality
- Low mean shear stress - High *FRS*	Low	- Diametrical changes with high opening angle inducing streamline separation - Downstream the curved edge of bends at low coil curvature[14]	High surface quality
- Low mean shear stress - Low *FRS*	Low	Confined zones (sudden contraction or expansion)[14]	High surface quality

and a gasket at the end of the pipe "f" induce a low clean ability level at the left section of zone 14, and for the entire zone 15. Asymmetric behavior of the flow appears clearly in zone 14 in cleanability experiments. Influence of the gasket zone on the cleanability is more important upstream, as shown by the comparison between zones 15 and 16. This is also clearly observed on the entire loop (both on horizontal and vertical lines). High disturbances induced by these surface irregularities is confirmed by high-fluctuating shear rates measured at P_{19} and P_{20} (60.9 and 71%).

Figure 8 shows that the flow establishment position after the bend corresponds to x/H = 54. In addition, wall shear stress values become nearer to the theoretical value for a fully developed flow (3.26 Pa) at the end of part "g". On the other hand, according to Rizk et al.[47] boundary layer growth, due to the flow establishment, induces the decrease of wall shear forces. Thus, zone 17 located under x/H = 54, exhibits high-shear stress, which explains the observed correctly cleanable level. Finally, same effects of the bend and surface irregularities as for the horizontal line are observed at zone 18 and explain the same cleanability level.

To summarize, the resistance to cleaning processes in the test loop is mainly governed by the adhesion strength of spores induced by the applied flow rate in the soiling step (e.g., the upper section of zone 8). Moreover, in some zones, the high-surface roughness parameters constitute deposit spots for spores (zones 9, 11 and 15). Thus, despite the high-wall shear stress values, spores removal is very difficult. Table 3 summarizes the shear stress forces effect on the cleanability levels for different geometries and surface properties.

Conclusions

Wall shear stress and velocity profile measurements allowed to explain the levels of adhering spores before and after cleaning of a section of a dairy production line consisting of geometrical changes like gradual asymmetric expansion or contraction pipes and bends.

The confined zone observed near the gradual expansion is characterized by low-mean and fluctuating shear stress values that explain their poor cleanability. Soiling experiments emphasize the role of recirculation zones in the potential adhesion of spores due to low-shear stress components. Indeed, the number of adhered spores at the surface depends on the wall shear stress which determines the adhesion forces magnitude. Moreover, transport of spores from the solution to the wall is a major parameter in the surface contamination depending on the flow rate. The beneficial effect of the recirculation zone on cleanability is very localized and decreases along with a weaker activity of the vortex. Experiments also showed that a homogeneous contamination or cleanability level could be obtained depending on the applied turbulence intensity at the straight section far from geometrical changes. Cleanability experiments emphasized that the gradual expansion presents low-cleanability level due to the fluid separation, which leads to flow disturbance. This result depends essentially on equipment design, in particular the opening angle of the gradual expansion and the bend coil curvature. These parameters must be selected in order not to disturb the flow and to induce streamline separation.

Electrochemical measurements showed that the limited flow disturbance with a nonboundary layer detachment from

the wall observed at gasket and welding zones induces the increase of the mean wall shear stress. However, cleanability analyses at different positions in the horizontal and the vertical lines showed that these zones constitute deposit spots for spores due to the high surface roughness. Despite the high-shear stress values generated by the applied flow, low-cleanability level is observed at these zones. In this case, cleanability is likely to be controlled by the surface roughness parameters, especially when the average roughness exceeds the standard value of 0.8 μm.[11] As a result, it is necessary to promote little disturbances of the boundary layer through straight pipes of important length. The use of progressive geometrical changes with small opening angle and high-surface quality could be proposed.

In future works, the determination of adhesion forces of *Bacillus cereus* spores is necessary to identify the critical force values controlling the alternation between the adhesion and the detachment of spores at the stainless steel surfaces.

Acknowledgments

This work was supported by the French Ministry of Agriculture in the framework of a program involving different partners (CETIM, Laval Mayenne Technopole, Lactalis R&D, Boccard - Division Alimentaire, Goavec Ingenierie, Pierre Guerin and Service Industriel Tuyauterie). This work was also made in the framework of an institutional collaboration between CNRS and INRA. Authors are very grateful to Hervé Datchoua, Jean Jacquemont, Jean-François Migdal and Jacky Six for their technical supports.

Notation

C = ultrasound velocity, m.s^{-1}
D = diffusion coefficient of the reacting species, m^2.s^{-1}
Dn = Dean number, $Re(r_0/r_c)$
f = emitted ultrasounds frequency, s^{-1}
f_D = Doppler frequency, s^{-1}
$f(z^+)$ = correlation function
FRS = fluctuation shear rate, dimensionless
G = gasket zone
H = difference between the highest diameter and the lowest one in a loop, m
$I(t)$ = instantaneous limiting current, A
l_e = equivalent probe length, m
L^+ = dimensionless electrode length, l_eV^*/υ
l_e = sampling length, mm
Pe = Péclet number, dimensionless
P_t = profile depth, μm
R_a = average roughness, μm
r_c = bend coil radius, m
Re = Reynolds number, $2r_0V/\upsilon$
r_0 = pipe radius, m
$Sh(t)$ = Sherwood number, dimensionless
$S_{lev}(t)$ = wall shear stress using the "Levêque solution", (s^{-1})
$S_{sob}(t)$ = wall shear stress using Sobolik et al.[23] method, (s^{-1})
$\overline{S}$, $s(t)$ = average value and fluctuating velocity gradients, s^{-1}
$\overline{s^2}$ = fluctuating energy of shear rate (s^{-2})
Tu = turbulence intensity, dimensionless
V^* = friction velocity, m.s^{-1}
V, v, v' = average, instantaneous and fluctuating velocities, m.s^{-1}
$V_{\max}$ = maximum velocity for each profile, m.s^{-1}
x = axial coordinate, m
x/H = dimensionless axial length
y = radial coordinate of pipes, m
y/2 r_0 = dimensionless radial length
$Z(x)$ = roughness profile
Z^+ = dimensionless length, xV^*/υ
W = welding zone

Greek letters

Λ_{fz}^+ = integral correlation length, dimensionless
υ = kinematic viscosity, m^2.s^{-1}
η = dynamic viscosity of the fluid, Pa.s
θ = Doppler angle, rad
t = acquisition time, s
τ_w = mean wall shear stress, Pa

Literature Cited

1. Visser J, Jeurnink TJM. Fouling of heat exchangers in the dairy industry. *Exp Therm Fluid Sci*. 1997;14:407–424.
2. Imamura K, Kawasaki Y, Awadzu T, Sakiyama T, Nakanishi K. Contribution of acidic amino residues to the adsorption of peptides to a stainless steel surface. *J Colloid Interface Sci*. 2003;267:294–301.
3. Santos O, Nylander T, Paulsson M, Trägårdh C. Whey protein adsorption onto steel surfaces-effect of temperature, flow rate, residence time and aggregation. *J Food Eng*. 2006;74:468–483.
4. Hermanowicz SW, Danielson RE, Cooper RC. Bacterial deposition on and detachment from surfaces in turbulent flow. *Biotechnol Bioeng*. 1989;33:157–163.
5. Tauveron G, Slomianny C, Henry C, Faille C. Variability among *Bacillus cereus* strains in spore surface properties and influence on their ability to contaminate food surface equipment. *Int J Food Microbiol*. 2006;110:254–262.
6. Bouman S, Lund DB, Driessen FM, Schmidt DG. Growth of thermoresistant *Streptococci* and deposition of milk constituents on plates of heat exchangers during long operating times. *J Food Prot*. 1982;45:806–812.
7. Te Giffel MC, Beumer RR, Langeveld LPM, Rombouts FM. The role of heat exchangers in the contamination of milk with *Bacillus cereus* in dairy processing plants. *Int J Dairy Technol*. 1997;50:43–47.
8. Hüsmark U, Rönner U. The influence of hydrophobic, electrostatic and morphologic properties on the adhesion of *Bacillus* spores. *Biofouling*. 1992;5:335–344.
9. Faille C, Jullien C, Fontaine F, Bellon-Fontaine MN, Slomianny C, Bénézech T. Adhesion of *Bacillus* spores and *Escherichia coli* cells to inert surfaces: role of surface hydrophobicity. *Can. J. Microbiol*. 2002;48:728–738.
10. Peng JS, Tsai WC, Chou CC. Inactivation and removal of *Bacillus cereus* by sanitizer and detergent. *Int J Food Microbiol*. 2002;77:11–18.
11. Jullien C, Bénézech T, Carpentier B, Lebret V, Faille C. Identification of surface characteristics relevant to the hygienic status of stainless steel for the food industry. *J Food Eng*. 2002;56:77–87.
12. Grasshoff A. Hygienic design: The basis for computer controlled automation. *Trans IchemE, Part C, Food Bioprod Proc*. 1992;70:69–77.
13. Jensen BBB, Friis A, Bénézech T, Legentilhomme P, Lelièvre C. Local wall shear stress variations predicted by computational fluid dynamics for hygienic design. *Trans IchemE, Part C, Food Bioprod Proc*. 2005;83:1–8.
14. Blel W, Bénézech T, Legentilhomme P, Legrand J, Le Gentil-Lelièvre C. Effect of flow arrangement on the removal of *Bacillus* spores from stainless steel equipment surfaces during a cleaning in place procedure. *Chem Eng Sci*. 2007;62:3798–3808.
15. Lelièvre C, Legentilhomme P, Gaucher C, Legrand J, Faille C, Bénézech T. Cleaning in place: effect of local wall shear stress variation on bacterial removal from stainless steel equipment. *Chem Eng Sci*. 2002;57:1287–1297.
16. Jensen BBB, Friis A. Predicting the cleanability of mix-proof valves by use of wall shear stress. *J Food Process Eng*. 2005;28(2):89–106.
17. Vujičić M, Crnojević C. Calculation of the separation point for the turbulent flow in plane diffusers. *Facta Universitatis, Series: Mechanics, Automatic Control and Robotics*. 2003;3(15):1001–1006.
18. Braga EJ, De Lemos MJS. Numerical simulation of turbulent flow in small angle diffusers and contractions using a new wall treatment

and a linear high Reynolds κ-ε model. *Num Heat Transfer, Part A*. 2004;45:911–933.
19. Midoux N. *Mécanique et rhéologie des fluides en génie chimique*. Paris, France; 1993. Lavoisier Tech Doc.
20. Reiss LP, Hanratty TJ. An experimental study of the unsteady nature of the viscous sublayer. *AIChE J*. 1963;8:154–160.
21. Labraga L, Lagraa B, Mazouz A, Keirsbulck L. Propagation of shear-layer structures in the near-wall region of a turbulent boundary layer. *Exp Fluids*. 2002;33:670–676.
22. Rehimi F, Aloui F, Ben Nasrallah S, Doubliez L, Legrand J. Inverse method for electrodiffusional diagnostics of flows. *Int J Heat Mass Transfer*. 2006;49:1242–1254.
23. Sobolik V, Wein O, Cermak J. Simultaneous measurement of film thickness and wall shear stress in wavy flow of non-Newtonian liquids. *Collection Czechoslovak Chem. Commun*. 1987;52:913–928.
24. Hanratty TJ, Campbell JA. *Measurement of wall shear stress, in Fluid Mechanics Measurements*. Goldstein RJ, ed. Hemisphere, Washington, DC; 1982;559–615.
25. Deslouis C, Huet F, Robin S, Tribollet B. Spectral analysis of wall turbulence with photolithography devised electrochemical probe. *Int J Heat Mass Transfer*. 1993;36:823–829.
26. Uberoi MS, Kovasznay LSG. On mapping and measurement of random fields. *Appl Math*. 1953;10:375–393.
27. Brodkey BS, Hershey HC. Transport Phenomena. A Unified Approach. *McGraw-Hill College*; 1988.
28. Takeda Y. Velocity profile measurement by ultrasonic Doppler method. *Exp Therm Fluid Sci*. 1995;10:444–453.
29. Wang T, Wang J, Ren F, Jin Y. Application of Doppler ultrasound velocimetry in multiphase flow. *Chem Eng J*. 2003;92:111–122.
30. Hüsmark U, Bénézech T, Faille C, Rönner U. *Bacillus* spores and molding with TTC AGAR: A useful method for the assessment of food processing equipment cleanability. *Biofouling*. 1999;14:15–24.
31. Bénézech T, Lelièvre C, Membré JM, Viet A-F, Faille C. A new method for in-place cleanability of food processing equipment. *J Food Eng*. 2002;54:7–15.
32. International Organisation for Standardisation, ISO 4288. Geometrical Product Specifications (GPS). Surface texture: Profile method - Rules and procedures for the assessment of surface texture. *AFNOR*. 1998;E05–054.
33. Idelcik IE. *Memento des pertes de charge*. Paris, France: Eyrolles. 1960.
34. Legrand J, Aouabed A, Legentilhomme P, Lefèbvre G, Huet F. Use of electrochemical sensors for the determination of wall turbulence characteristics in annular swirling flow. *Exp Therm Fluid Sci*. 1997;15:125–136.
35. Dabros T, Adamczyk Z. Non-inertial particle transfer to the rotating disk under an external force field (laminar flow). *Chem Eng Sci*. 1979;34:1041–1049.
36. Dickinson RB, Cooper SL. Analysis of shear-dependent bacterial adhesion kinetics to biomaterial surfaces. *AIChE J*. 1995;41:2160–2174.
37. Lelièvre C, Antonini G, Faille C, Bénézech T. Cleaning-in-place, modeling of cleaning kinetics of pipes soiled by *Bacillus* spores assuming a process combining removal and deposition. *Trans. IchemE, Part C, Food Bioprod Proc*. 2002;80:305–311.
38. Rutter PR, Vincent B. Attachment mechanisms in the surface growth of microorganisms. Bazin, JI. Prosser, eds. *Physiological models in microbiology*. Boca Raton, FL: CRC Press; 1988;2:87–107
39. Elimelech M. Particle deposition on ideal collectors from dilute flowing suspensions: mathematical formulation, numerical solution, and simulations. *Sep Technol*. 1994;4:186–212.
40. Korber DR, Lawrence JR, Zhang L, Caldwell DE. Effect of gravity on bacterial deposition and orientation in laminar flow environments. *Biofouling*. 1990;2:335–350.
41. De Jong P, Te Giffel MC, Kiezebrink EA. Prediction of the adherence, growth and release of microorganisms in production chains. *Int J Food Microbiol*. 2002;74:13–25.
42. Roosjen A, Boks NP, van der Mei HC, Busscher HJ, Norde W. Influence of shear on microbial adhesion to PEO-brushes and glass by convective - diffusion and sedimentation in a parallel plate flow chamber. *Colloids Surfaces B: Biointerfaces*. 2005;46:1–6.
43. Faille C, Dennin L, Bellon-Fontaine MN, Bénézech T. (1999), Cleanability of stainless steel surfaces soiled by *B. Thuringiensis* spores under various flow conditions. *Biofouling*. 1999;14(2):143–151.
44. Ziskind G, Fichman M, Gutfinger C. Resuspension of particulates from surfaces to turbulent flows - review and analysis. *J Aerosol Sci*. 1995;26:613–644.
45. Ziskind G, Fichman M, Gutfinger C. Adhesion moment model for estimating particle detachment from a surface. *J Aerosol Sci*. 1997;28:623–634.
46. Cleaver JW, Yates B. Mechanism of detachment of colloidal particles from a flat substrate in a turbulent flow. *J Colloid Interface Sci*. 1973;44:464–473.
47. Rizk TY, Thompson GE, Dawson JL. Mass transfer enhancement associated with sudden flow expansion. *Corrosion Sci*. 1996;38(10):1801–1814.

Manuscript received Oct. 10, 2007, and revision received Apr. 21, 2008.